Aeromechanics Analysis of a Compound Helicopter

Hyeonsoo Yeo

Aeroflightdynamics Directorate (AMRDEC)
U.S. Army Research, Development, and Engineering Command
Ames Research Center, Moffett Field, California

Wayne Johnson

Flight Vehicle Research and Technology Division
NASA Ames Research Center
Moffett Field, California

Abstract

A design and aeromechanics investigation was conducted for a 100,000-lb compound helicopter with a single main rotor, which is to cruise at 250 knots at 4000 ft/95 deg F condition. Performance, stability, and control analyses were conducted with the comprehensive rotorcraft analysis CAMRAD II. Wind tunnel test measurements of the performance of the H-34 and UH-1D rotors at high advance ratio were compared with calculations to assess the accuracy of the analysis for the design of a high speed helicopter. In general, good correlation was obtained with the increase of drag coefficients in the reverse flow region. An assessment of various design parameters (disk loading, blade loading, wing loading) on the performance of the compound helicopter was made. Performance optimization was conducted to find the optimum twist, collective, tip speed, and taper using the comprehensive analysis. Blade twist was an important parameter on the aircraft performance and most of the benefit of slowing the rotor occurred at the initial 20 to 30% reduction of rotor tip speed. No stability issues were observed with the current design and the control derivatives did not change much with speed, but did exhibit significant coupling.

Notation

A	rotor disk area
C_L	rotor lift coefficient
C_{Pi}	rotor induced power coefficient
C_{Po}	rotor profile power coefficient
C_T	rotor thrust coefficient
C_W	rotor weight coefficient
D/q	airframe drag divided by dynamic pressure
L/D = WV/P	aircraft effective lift-to-drag ratio
M	Mach number
M_{at}	advancing tip Mach number
P	aircraft power
R	rotor radius
S	wing area
V	flight speed
W	gross weight
W/A	disk loading
W/S	wing loading
α_s	shaft tilt angle
α_w	wing incidence angle
μ	advance ratio
σ	solidity (thrust weighted)
DL	disk loading
WL	wing loading

Presented at the American Helicopter Society 62nd Annual Forum, Phoenix, Arizona, May 9-11, 2006.

Introduction

Recently, the NASA Heavy Lift Rotorcraft Systems Investigation was conducted to identify candidate configurations for a large civil VTOL transport that is technically promising and economically competitive [1]. The vehicle is required to carry 120 passengers over a range of 1200 nautical miles and cruise at 350 knots at an altitude of 30,000 ft. A large civil tandem compound (LCTC) helicopter was designed as one of the candidate configurations to meet this NASA 15-year notional capability [2]. This study also revealed the need to further investigate the aeromechanics issues of a compound helicopter.

The compound helicopter is a method of achieving high speed capability while retaining the hover advantages of a helicopter. The compound helicopter is defined as a helicopter with both a wing and auxiliary propulsion. In general, the lifting and propulsive force capabilities of a helicopter rotor decrease with forward speed as a result of asymmetric flow conditions encountered by the rotor. The compound helicopter circumvents these limits by sharing lift between the wing and rotor as well as eliminating the need for rotor propulsive force. To maintain low rotor drag at high speed, it is necessary to slow the rotor, in part to minimize the compressible drag rise on the advancing blade.

In this paper, a design and aeromechanics investigation

Report Documentation Page

Form Approved
OMB No. 0704-0188

1. REPORT DATE	2. REPORT TYPE	3. DATES COVERED
MAY 2006		**00-00-2006 to 00-00-2006**

4. TITLE AND SUBTITLE	5a. CONTRACT NUMBER
Aeromechanics Analysis of a Compund Helicopter	5b. GRANT NUMBER
	5c. PROGRAM ELEMENT NUMBER
6. AUTHOR(S)	5d. PROJECT NUMBER
	5e. TASK NUMBER
	5f. WORK UNIT NUMBER
7. PERFORMING ORGANIZATION NAME(S) AND ADDRESS(ES) **US Army Aviation and Missile Command,Army/NASA Rotorcraft Division,Army Aeroflightdynamics Directorate (AMRDEC),Moffett Field,CA,94035**	8. PERFORMING ORGANIZATION REPORT NUMBER
9. SPONSORING/MONITORING AGENCY NAME(S) AND ADDRESS(ES)	10. SPONSOR/MONITOR'S ACRONYM(S)
	11. SPONSOR/MONITOR'S REPORT NUMBER(S)

12. DISTRIBUTION/AVAILABILITY STATEMENT
Approved for public release; distribution unlimited

13. SUPPLEMENTARY NOTES

14. ABSTRACT
see report

15. SUBJECT TERMS

16. SECURITY CLASSIFICATION OF:			17. LIMITATION OF ABSTRACT	18. NUMBER OF PAGES	19a. NAME OF RESPONSIBLE PERSON
a. REPORT **unclassified**	b. ABSTRACT **unclassified**	c. THIS PAGE **unclassified**	**Same as Report (SAR)**	**16**	

was conducted for a 100,000-lb compound helicopter with a single main rotor, which is to cruise at 250 knots at 4000 ft/95 deg F condition (Fig. 1). In contrast, the LCTC (Ref. 2) was designed for much higher speed and altitude. This paper presents the rotor performance correlation at high speed and the results of the compound helicopter design investigation. A parametric study was conducted to understand the effects of design parameters on the performance of the aircraft. Stability and control issues are also investigated.

CAMRAD II Modeling

Performance, loads, and stability analyses were conducted with the comprehensive rotorcraft analysis CAMRAD II [3]. CAMRAD II is an aeromechanics analysis of rotorcraft that incorporates a combination of advanced technologies, including multibody dynamics, nonlinear finite elements, and rotorcraft aerodynamics. The trim task finds the equilibrium solution for a steady state operating condition, and produces the solution for performance, loads, and vibration. The flutter task linearizes the equations about the trim solution, and produces the stability results. The aerodynamic model includes a wake analysis to calculate the rotor nonuniform induced-velocities, using rigid, prescribed, or free wake geometry. CAMRAD II has undergone extensive correlation of performance and loads measurements on helicopters [4–6].

A complete aeroelastic model was developed for the analysis of the compound helicopter. The comprehensive analysis modeled the auxiliary propulsion as forces applied to the airframe. Rotor/wing interference was accounted for using a vortex wake model for both the rotor and the wing. For all the calculations made in this study, an elastic blade model was used, scaled from the LCTC blade design. Rotor performance was calculated using nonuniform inflow with prescribed wake geometry in high speed cruise and free wake geometry in hover.

In cruise, the aircraft was trimmed using lateral stick to the ailerons, longitudinal stick to the elevator, pedal to differential propeller thrust; plus propeller thrust, and aircraft pitch and roll angles. Rotor collective pitch angle was set to values optimized for cruise performance (optimized rotor thrust). In addition to three force and three moment equilibrium of the aircraft, rotor hub roll and pitch moment were trimmed to zero (for load control) using rotor cyclic pitch; thus there were eight trim variables for cruise.

Rotor Performance Correlation at High Speed

The ability to accurately predict the performance of a helicopter is essential for the design of future rotorcraft. It is necessary to assess the accuracy and reliability of these prediction methods, with the ultimate goal of providing the technology for timely and cost-effective design and development of new rotors.

Wind tunnel test data of the full-scale H-34 rotor [7] and UH-1D rotor [8] obtained in the late 1960's provide a set of test conditions at high advance ratios. A full-scale H-34 articulated rotor with zero twist blades was tested in the NASA Ames 40- by 80-Foot Wind Tunnel. Tunnel speed and rotor rotational speed were adjusted to obtain the desired advance ratio and advancing tip Mach number. At each combination of shaft tilt angle and collective pitch, the cyclic pitch was adjusted to minimize first harmonic blade flapping. A full-scale UH-1D teetering rotor blades reduced in diameter to 34 feet were tested in the NASA Ames 40- by 80-Foot Wind Tunnel. The test procedure was same as for the H-34 rotor test. Both rotors used an NACA 0012 airfoil.

Rotor performance calculations with CAMRAD II were compared with the wind tunnel test data in Figs. 2 and 5. Figure 2 shows the rotor induced power plus profile power versus rotor lift for the H-34 rotor for three different shaft tilt angles. Rotor performance was calculated using nonuniform inflow with free wake geometry and unsteady aerodynamics, but a dynamic stall model was not used. The rotor induced plus profile power increases as advance ratio increases for the same rotor lift and as rotor lift increases for the same advance ratio. The analysis shows, in general, good correlation with the measurements. Underprediction of rotor power at high rotor lift was observed. It appears that the current analysis (or airfoil table used) has optimistic stall characteristics.

The good correlation in Fig. 2 was obtained with drag coefficient change in the NACA 0012 airfoil table. Figure 3 shows the effect of airfoil drag coefficient on the H-34 rotor performance at α_s = 0 deg. The analysis with the existing NACA 0012 airfoil table shows good correlation at μ = 0.46. However, the analysis underpredicted the required power at higher advance ratios and the underprediction became larger as the advance ratio increases. This trend appears to be lower drag coefficients in the reverse flow region, because the reverse flow region increases proportional to μ^2. The drag coefficients of the airfoil table were uniformly increased by 0.1 in the reverse flow region ($-180 \leq \alpha \leq -90$, $90 \leq \alpha \leq 180$), resulting in significantly better correlation. The actual airfoil drag characteristics in the reverse flow region are undoubtedly more complicated than implied by this simple correction. In particular, a

strong dependence on Mach number is likely. In the NACA 0012 airfoil table used, there is no dependence on Mach number in the reverse flow region.

Figure 4 shows the effect of wake modeling on the H-34 rotor performance at α_s = 0 deg. Rotor performance was calculated with prescribed wake geometry and the result was compared with that with free wake geometry. The wake is quickly convected from the rotor disk in high speed condition. Thus, there is no difference in the rotor performance calculations between the two wake geometries.

Figure 5 shows the rotor induced power plus profile power versus rotor lift for the UH-1D rotor for three different shaft tilt angles. Again, the drag coefficients of the NACA 0012 airfoil were uniformly increased by 0.1 in the reverse flow region. The analysis shows reasonably good correlation, considering the scatter of the measured data. There is an underprediction of rotor power at μ = 0.65, although the same trend was not observed at μ = 0.51 and 0.76. The reason for the observed difference is not known at present.

For conventional helicopters, the reverse flow region does not have a significant influence on the rotor performance because of moderate cruise speed and low dynamic pressure in the region. However, high speed helicopters, such as the 250 knot compound helicopter studied in this paper, have received more attention recently. Therefore, the airfoil characteristics in the reverse flow region need to be throughly studied and validated.

Aircraft Design Study

An assessment of various compound helicopter designs was made in order to understand the effects of design parameters on the performance of the aircraft and to define a baseline model. The compound helicopter configuration developed in this study is shown in Fig. 1. The aircraft has a six bladed rotor, a high wing, a horizontal tail, and two auxiliary propellers located on the wings for cruise propulsion and anti-torque in hover. State-of-the-art rotor airfoils (VR-12 and SSCA09) were used.

A hingeless rotor hub was used. Blade inertial and structural properties were scaled from the blade developed from the LCTC [2]. Figure 6 shows the calculated blade frequencies, at a collective pitch angle of 10 deg. At helicopter-mode tip speeds, the flap frequency was about 2.3/rev, the lag frequency was above 5.4/rev and the torsion frequency about 6.5/rev.

Table 1 shows the design parameters investigated. The baseline aircraft design parameters (Fig. 1) are a disk loading of W/A = 15 lb/ft^2, blade loading of C_T/σ = 0.14, and wing loading of W/S = 100 lb/ft^2. This design was the design optimum for the LCTC, and is shown below to give good performance for the present aircraft. C_T/σ = 0.14 and W/S = 100 are appropriate for an aircraft that unloads the rotor at a relatively low speed. The aircraft drag is D/q = 40.5 ft^2. The baseline design has a wing span equal to the rotor diameter (Fig. 1). The hover tip speed is 750 ft/sec, and the cruise tip speed gives M_{at} = 0.8 at 250 knots. The advance ratio is then μ = 0.84 at 250 knots.

Design variations of disk loading (W/A = 15 vs 12), blade loading (C_T/σ = 0.14 vs 0.09), and wing loading (W/S = 100 vs 120) were examined. The larger disk area will give lower hover power. The larger blade area or smaller wing area correspond to loading the rotor rather than the wing. Note that C_T/σ = 0.09 would be appropriate for an advanced technology helicopter, hence the rotor could carry the aircraft weight to conventional helicopter speeds. The calculated performance results are presented in Figs. 7 through 10, all for the design cruise condition of 250 knots. For each combination of the disk loading, design blade loading, and wing loading, three collective angles (-3, 0, and 3 deg) and six values for the difference between wing incidence and shaft tilt angle ($\alpha_w - \alpha_s$ = -4, -1, 1, 3, 5, and 7 deg) were used. The rotor tip RPM was 103.0 to obtain M_{at} = 0.8.

Figure 7 shows the aircraft lift-to-drag ratio. Higher design blade loading (smaller blade chord) increased the aircraft lift-to-drag ratio, but higher wing loading (smaller wing area) reduced the aircraft lift-to-drag ratio. Disk loading has a small influence on the aircraft performance, although it will have an impact on the rotor weight. In general, the best performance is obtained for the collective angle of 0 or -3 deg and $\alpha_w - \alpha_s$ = 3 deg at each combination of disk loading, design blade loading, and wing loading.

Figures 8 and 9 show the rotor and wing lift, respectively. As the $\alpha_w - \alpha_s$ increases, the rotor lift decreases and wing lift increases. The higher collective angle increases the rotor lift and decreases wing lift. The optimum lift sharing between the rotor and wing varied depending on the disk loading, design blade loading, and wing loading. The rotor needs to carry more lift as the wing loading increases and the design blade loading decreases. The rotor carries 8.8% of the aircraft gross weight for the disk loading of 15, design blade loading of 0.14, and wing loading of 100 (Fig. 8(a)), and 14.1% of the aircraft gross weight for the disk loading of 12, design blade loading of 0.09, and wing loading of 120 (Fig. 8(h)).

Figure 10 shows the rotor shaft power. The rotor power increases as $\alpha_w - \alpha_s$ increases. The rotor power increases

as the design blade loading increases and decreases as the wing loading increases. The required rotor power at the optimum aircraft lift-to-drag ratio occurred with a small, positive shaft power to the rotors: between 500 and 1000 HP. With the rotor in autorotation (zero rotor shaft power), the rotor thrust was large, hence the total rotor drag larger and the aircraft L/D somewhat smaller.

Rotor Parametric Study

This section describes a parametric study of key rotor design parameters conducted with the comprehensive analysis. The baseline design was the disk loading of 15, design blade loading of 0.14, wing loading of 100, collective angle of 0 deg, and $\alpha_w - \alpha_s$ of 3 deg.

The blade twist was varied to optimize the rotor for hover and cruise performance. The hover condition was 750 ft/sec tip speed, C_T/σ = 0.149 (6% download). The cruise condition was 250 knots, 501.7 ft/sec tip speed. The twist distribution had two linear segments, inboard (0.0R to 0.5R) and outboard (0.5R to 1.0R). Figure 11 presents the results for twist optimization. For each value of outboard twist (-15, -12, -9, -6, -3, and 0 deg), the inboard twist values are -3, 0, 3, and 6 deg. A large negative twist improves hover performance, but the zero twist gives the best cruise performance. The optimum twist of 0 deg inboard and -12 deg outboard was selected based on the hover-cruise compromise. The result shows larger variations of the figure of merit and aircraft L/D for the current design than those for the LCTC developed in the NASA Heavy Lift Investigation as shown in Fig. 12. Thus, the blade twist is more important parameter for the the current design than the LCTC. However, the the aircraft L/D has less sensitive to the inboard twist change for fixed outboard twist. Thus, the benefit of bi-linear twist diminished for the current design compared with the LCTC.

The rotor advancing tip Mach number was varied from 0.5 to 0.9 to investigate the effects of the rotor rotational speed on the high speed cruise performance, as shown in Fig. 13. To maintain low rotor drag at high speed, it is necessary to slow the rotor. The aircraft lift-to-drag ratio increases as the advancing tip Mach number decreases, reaching the maximum at M_{at} = 0.55, which corresponds to μ = 1.98. Most of the benefit of slowing the rotor occurs at the initial 20 to 30% reduction of rotor tip speed. The design point was found at M_{at} = 0.80, which corresponds to μ = 0.84.

The blade taper was varied as shown in Fig. 14. The taper model considered was constant thrust-weighted solidity (chord at 75%R). The aircraft L/D decreased as the taper was reduced. Although the taper of 1.0 produced the best aircraft L/D, the taper of 0.8 (tip/root chord) was selected to reduce the blade weight.

Collective pitch of the rotor was varied by 1 deg from -3 to +3 deg to further investigate the effect of the collective pitch (rotor thrust) on the aircraft lift-to-drag ratio, as shown in Fig. 15. The aircraft performance was not sensitive to the collective angle change. The highest aircraft lift-to-drag ratio, which occurred with the -2 deg collective angle, was 0.34% higher than that with the baseline collective angle (0 deg). The aircraft lift-to-drag ratio changed less than 2% with the collective angles investigated.

Good rotor performance correlation was obtained for the H-34 and UH-1D rotor with the increased drag coefficients of the NACA 0012 airfoil table at high advance ratios. Most of helicopter airfoil tables have similar drag coefficients as the NACA 0012 airfoil in the reverse flow region. Figure 16 shows the effect of the airfoil drag coefficients on the compound helicopter performance. The drag coefficients in the reverse flow region were increased by 0.1, same as the NACA 0012 airfoil case. The aircraft lift-to-drag ratio was reduced by about 6% with the increased drag coefficients at all $\alpha_w - \alpha_s$ investigated.

Stability and Control

Stability and control are among the most important aspects of the design of helicopters. Stability and control of a compound helicopter are investigated using the baseline design as the disk loading of 15, design blade loading of 0.14, wing loading of 100, collective angle of 0 deg, and $\alpha_w - \alpha_s$ of 3 deg.

Figure 17 shows rotor stability calculations in level flight. Rotor tip speed was varied linearly from the hover value at 0 knots to the cruise value at 250 knots. The corresponding blade frequencies are shown in Fig. 6. Stability is, in general, insensitive to the speed. No stability issues were observed between 150 to 300 knots.

Figure 18 shows rotor stability with respect to flap frequency change at 250 knots. In this calculation, a flap hinge and spring stiffness were introduced to change the flap frequency to that of a conventional articulated rotor. The hingeless rotor blade was simulated with very stiff spring and the spring stiffness was decreased to reduce flap frequency. The baseline blade, which was scaled from the LCTC blade design, shows stable modes with the flap frequency change, as shown in Fig. 18(a). Blade lag and torsion stiffness were reduced by 75% from the baseline blade and the same analyais was conducted. The lag frequency became 4.03/rev and torsion frequency

became 4.89/rev at the cruise rotor speed. These frequency change significantly reduced stability margin, although all the modes were stable. Even with the reduced stiffness, the lag frequency was still higher than that of conventional helicopters (still above 2/rev at hover tip speed). A further study is required to examine the stability characteristics of a compound helicopter with more conventional blade frequency placements.

Helicopter control requires the ability to produce forces and moments on the vehicle. The changes of hub forces and moments with respect to pilot controls are shown in Fig. 19 as a function of flight speed, using the same rotor speed variation as for the stability calculations. The calculation was carried out for fixed controls, with $\pm$ 1 deg of collective and cyclic angle change relative to the trimmed solution. The phase shift needed for hingeless rotor control was not considered: longitudinal and lateral cyclic are not sine and cosine harmonics of root pitch. Figures 19(a) and 19(b) show the hub force and moment change with respect to collective angle change. As expected, collective angle changed vertical force by about 8000 to 12,000 lb at 175 and 300 knots, respectively. Lateral and longitudinal force change was small. A large roll moment change was observed. It is because the lift increase with the increased collective angle is concentrated on the advancing side due to a large reverse flow region on the retreating side.

Figures 19(c) and 19(d) show the hub force and moment change with respect to lateral cyclic angle change. Hub force change was small. There is a large pitch moment change, as expected.

Figures 19(e) and 19(f) show the hub force and moment change with respect to longitudinal cyclic angle change. The results are quite similar to the hub force and moment change with respect to collective angle. There are smaller changes in vertical force and roll moment with the longitudinal cyclic change than the collective change.

In summary, for this hingeless rotor the control derivatives did not change much with speed, but did exhibit significant coupling.

Conclusions

A design and aeromechanics investigation was conducted for a 100,000 lb compound helicopter with a single main rotor, which is to cruise at 250 knots at 4000 ft/95 deg F condition. Performance, stability, and control analyses were conducted with the comprehensive rotorcraft analysis CAMRAD II.

Wind tunnel test measurements of the performance of the H-34 and UH-1D rotors at high advance ratio were compared with calculations to assess the accuracy of the analysis for the design of a high speed helicopter. In general, good correlation was obtained when using increased drag coefficients in the reverse flow region.

An assessment of various design parameters (disk loading, design blade loading, wing loading) on the performance of the compound helicopter were made. A parametric study was conducted to investigate the effects of twist, collective, tip speed, taper, and drag coefficients on the aircraft L/D. Blade twist is a more important parameter on the aircraft performance for the current compound helicopter design than the tandem compound helicopter developed in the NASA Heavy Lift Investigation. The analysis showed that most of the benefit of slowing the rotor occurred at the initial 20 to 30% reduction of rotor tip speed.

No stability issues were observed with the current design and the control derivatives did not change much with speed, but did exhibit significant coupling.

References

[1] Johnson, W., Yamauchi, G. K., and Watts, M. E., "Design and Technology Requirements for Civil Heavy Lift Rotorcraft," Proceedings of the American Helicopter Society Vertical Lift Aircraft Design Conference, San Francisco, CA, January 2006.

[2] Yeo, H., and Johnson, W., "Aeromechanics Analysis of a Heavy Lift Slowed-Rotor Compound Helicopter," Proceedings of the American Helicopter Society Vertical Lift Aircraft Design Conference, San Francisco, CA, January 2006.

[3] Johnson, W., "Technology Drivers in the Development of CAMRAD II," American Helicopter Society Aeromechanics Specialist Meeting, San Francisco, CA, January 1994.

[4] Yeo, H., Bousman, W. G., and Johnson, W., "Performance Analysis of a Utility Helicopter with Standard and Advanced Rotor," *Journal of the American Helicopter Society*, Vol. 49, No. 3, July 2004.

[5] Yeo, H., and Johnson, W., "Assessment of Comprehensive Analysis Calculation of Airloads on Helicopter Rotors," *Journal of Aircraft*, Vol. 42, No. 5, September-October 2005.

[6] Yeo, H., and Johnson, W., "Comparison of Rotor Structural Loads Calculated Using Comprehensive Analysis," Proceedings of the 31st European Rotorcraft Forum, Florence, Italy, September 2005.

[7] McCloud, J. L., Biggers, J. C., and Stroub, R. H., "An Investigation of Full-Scale Helicopter Rotors at High Advance Ratios and Advancing Tip Mach Numbers," NASA TN D-4632, July 1968.

[8] Charles, B. D., and Tanner, W. H., "Wind Tunnel Investigation of Semirigid Full-Scale Rotors Operating at High Advance Ratios," USAAVLABS TR 69-2, January 1969.

Table 1 Compound helicopter sizing model

Operating condition (ft, deg)	4k/95	4k/95	4k/95	4k/95
Cruise speed (knots)	250	250	250	250
Mission GW (lb)	100,000	100,000	100,000	100,000
Disk loading W/A (lb/ft^2)	15	15	12	12
Rotor diameter (ft)	92.13	92.13	103.01	103.01
Tip speed, hover (ft/sec)	750	750	750	750
Tip speed, cruise (ft/sec)	502	502	502	502
Drag D/q (ft^2)	40.5	40.5	40.5	40.5
Drag, $(D/q)/(W/1000)^{2/3}$ (ft^2)	1.9	1.9	1.9	1.9
C_W/σ	0.14	0.09	0.14	0.09
Solidity	0.0992	0.1543	0.0794	0.1235
Number of blades	6	6	6	6
Chord (75%R, ft)	2.39	3.72	2.14	3.33
Taper ratio	0.8	0.8	0.8	0.8
Aspect ratio	19.25	12.38	24.06	15.47
Wing loading W/S (lb/ft^2)	100	120		
Area (ft^2)	1000	833		
Span (ft)	92.13	76. 78		
Chord (75%R, ft)	10.25	10.25		
Taper ratio	0.8	0.8		
Aspect ratio	8.49	7.07		

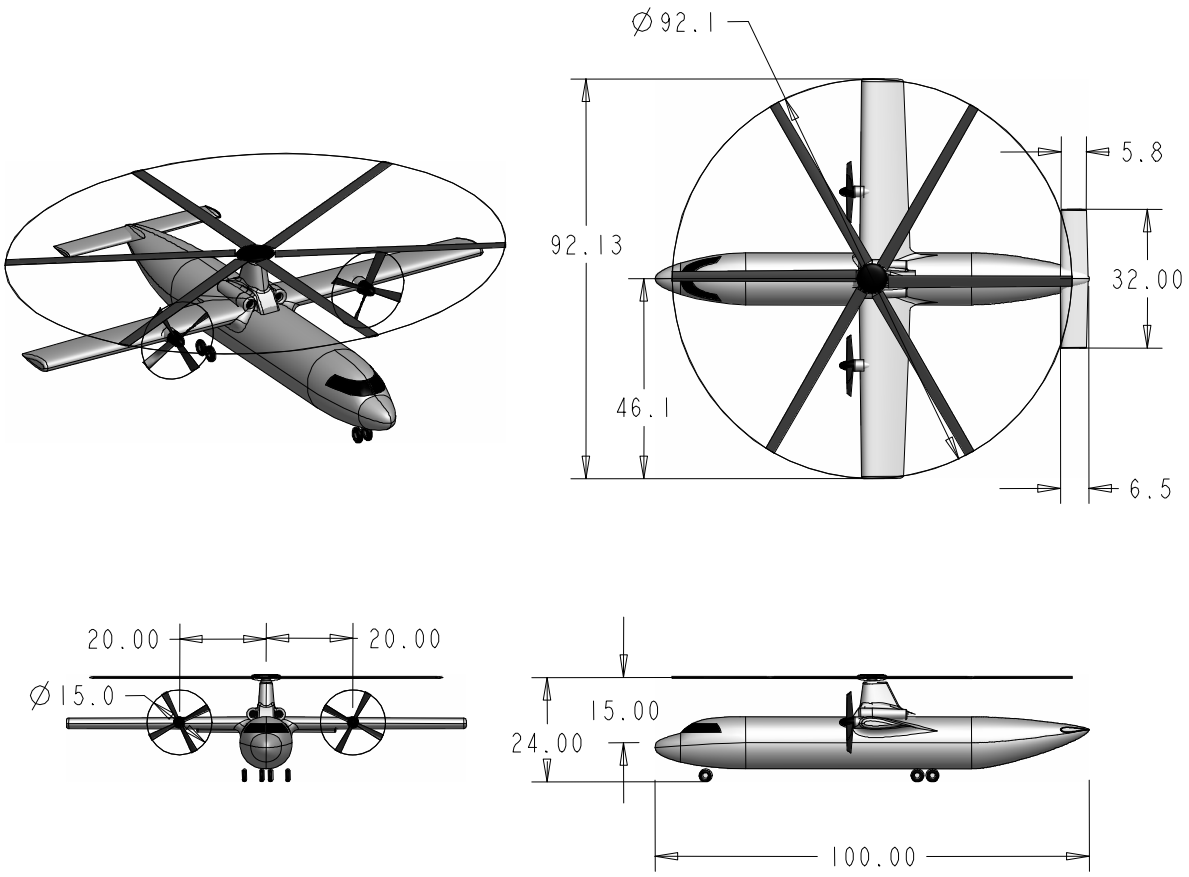

Fig. 1 Three-view of the compound helicopter - dimensions are in ft (courtesy Gerardo Nunez).

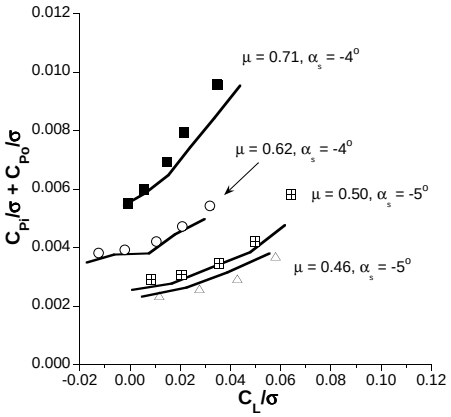

(a) around α_s = -5 deg

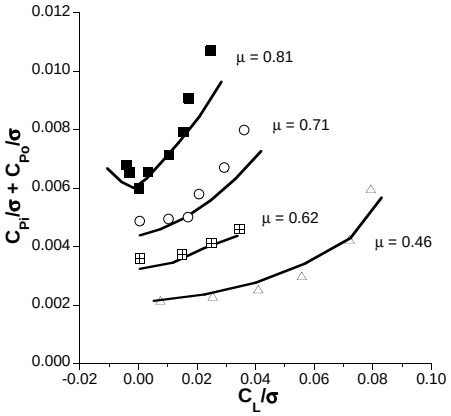

(b) α_s = 0 deg

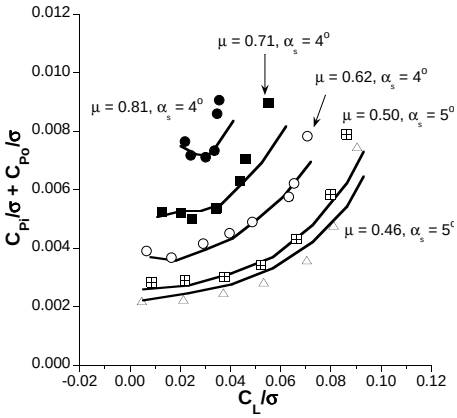

(c) around α_s = 5 deg

Fig. 2 H-34 rotor performance correlation (symbols: wind tunnel test, lines: analysis).

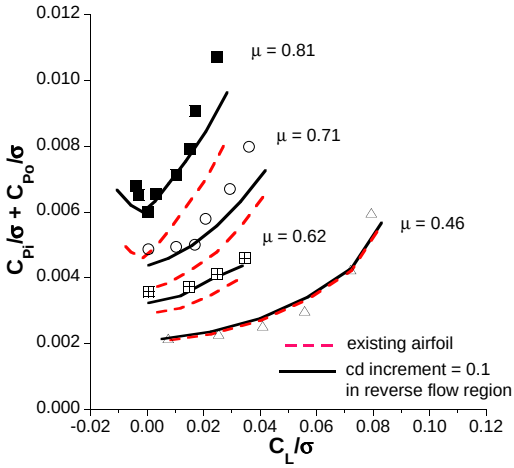

Fig. 3 Effect of airfoil drag coefficient on H-34 rotor performance at α_s = 0 deg (symbols: wind tunnel test, lines: analysis).

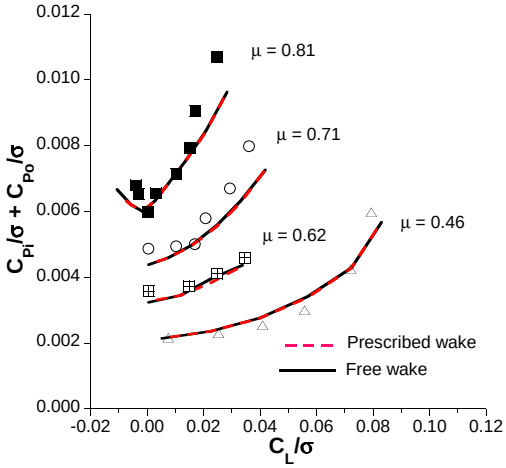

Fig. 4 Effect of wake modeling on H-34 rotor performance at α_s = 0 deg (symbols: wind tunnel test, lines: analysis).

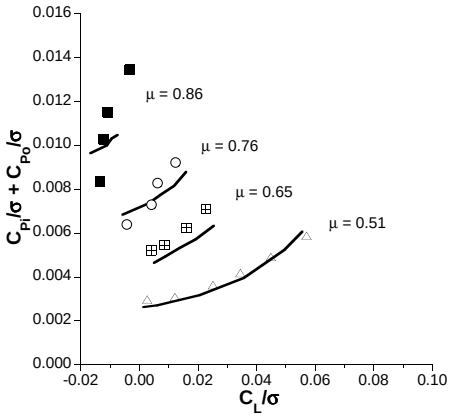

(a) α_s = -4 deg

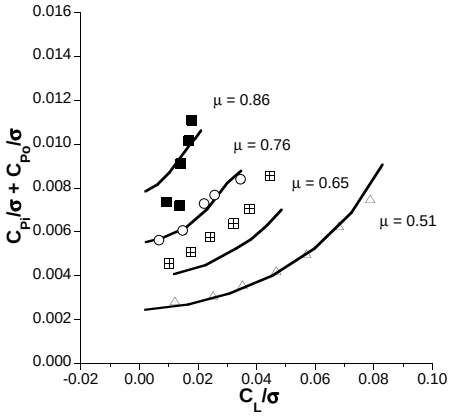

(b) α_s = 0 deg

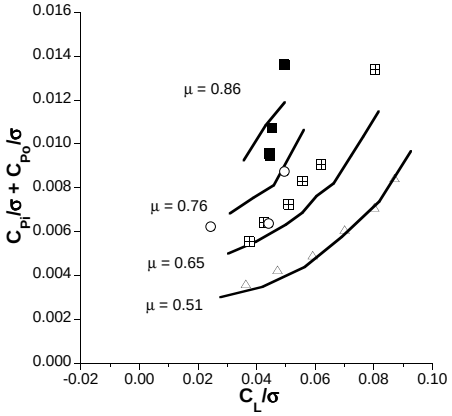

(c) α_s = 4 deg

Fig. 5 UH-1D rotor performance correlation (symbols: wind tunnel test, lines: analysis).

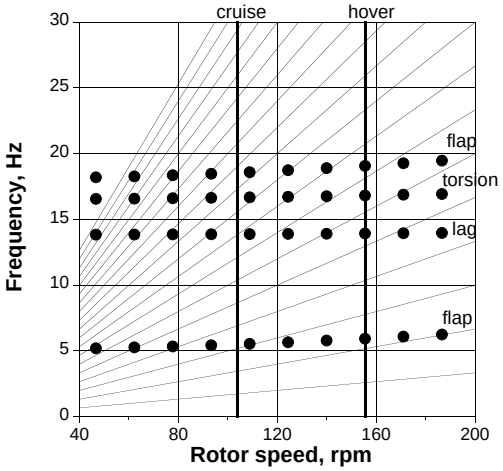

Fig. 6 Blade frequencies (collective = 10 deg).

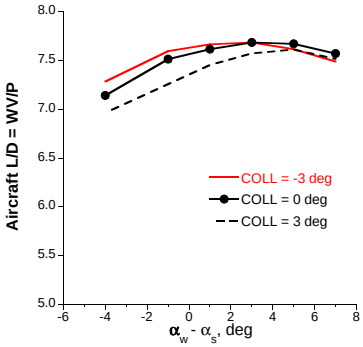

(a) DL = 15, C_W/σ = 0.14, WL = 100

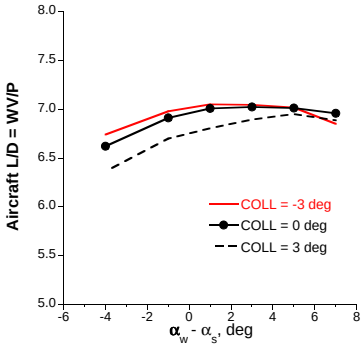

(b) DL = 15, C_W/σ = 0.14, WL = 120

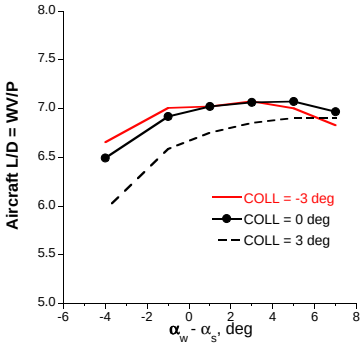

(c) DL = 15, C_W/σ = 0.09, WL = 100

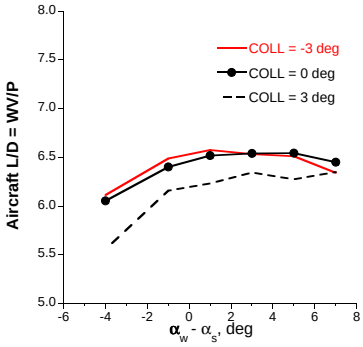

(d) DL = 15, C_W/σ = 0.09, WL = 120

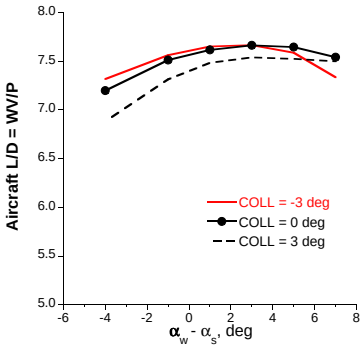

(e) DL = 12, C_W/σ = 0.14, WL = 100

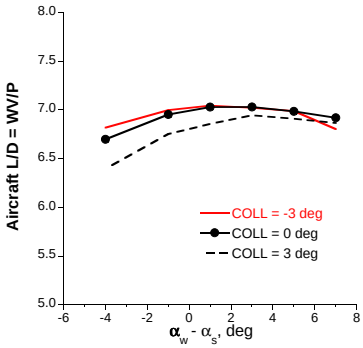

(f) DL = 12, C_W/σ = 0.14, WL = 120

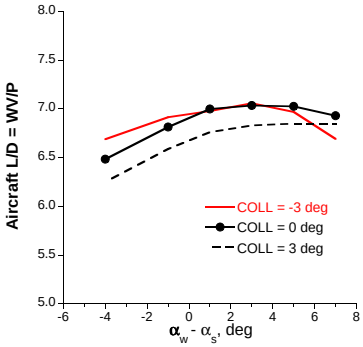

(g) DL = 12, C_W/σ = 0.09, WL = 100

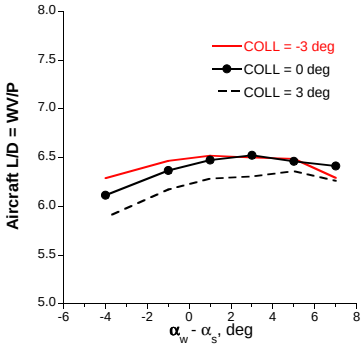

(h) DL = 12, C_W/σ = 0.09, WL = 120

Fig. 7 Aircraft lift-to-drag ratio.

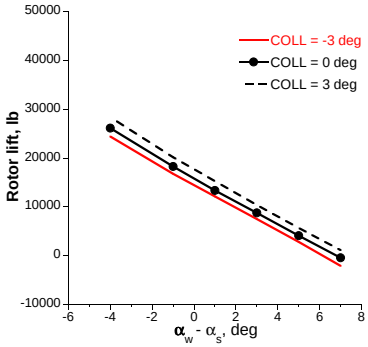

(a) DL = 15, C_W/σ = 0.14, WL = 100

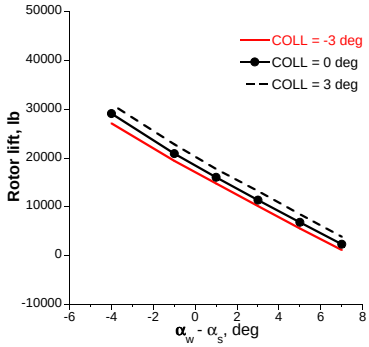

(b) DL = 15, C_W/σ = 0.14, WL = 120

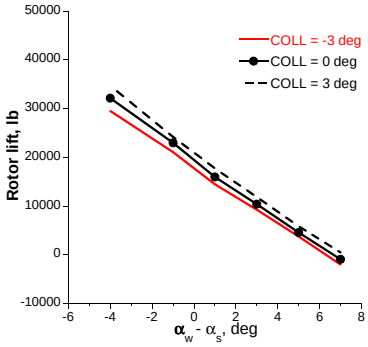

(c) DL = 15, C_W/σ = 0.09, WL = 100

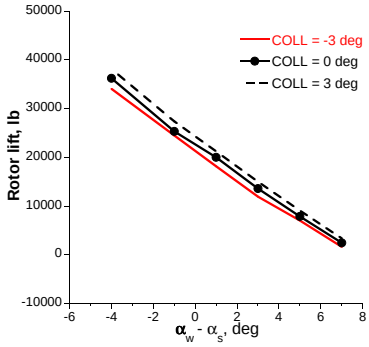

(d) DL = 15, C_W/σ = 0.09, WL = 120

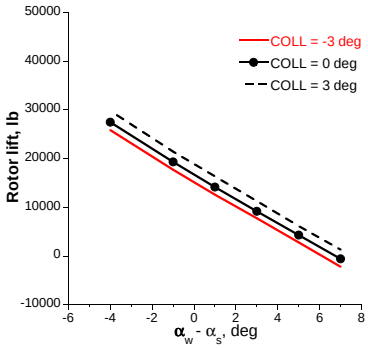

(e) DL = 12, C_W/σ = 0.14, WL = 100

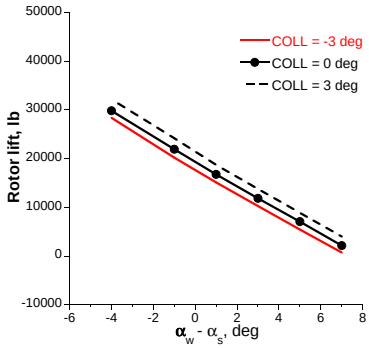

(f) DL = 12, C_W/σ = 0.14, WL = 120

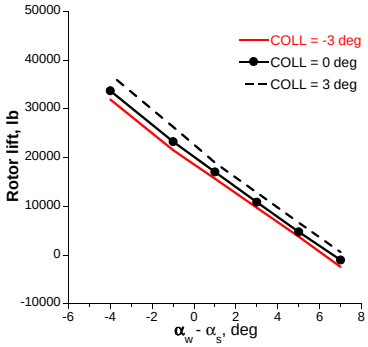

(g) DL = 12, C_W/σ = 0.09, WL = 100

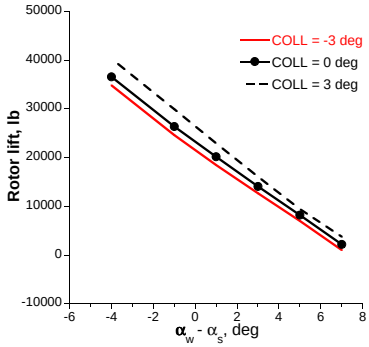

(h) DL = 12, C_W/σ = 0.09, WL = 120

Fig. 8 Rotor lift.

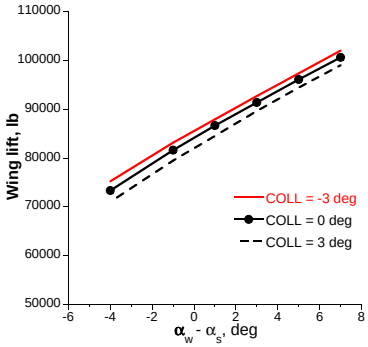

(a) DL = 15, C_W/σ = 0.14, WL = 100

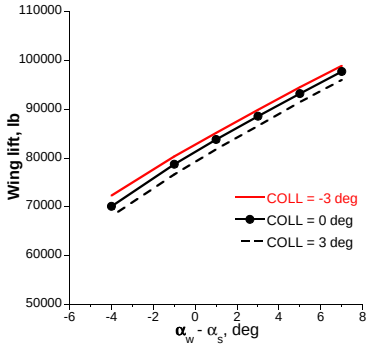

(b) DL = 15, C_W/σ = 0.14, WL = 120

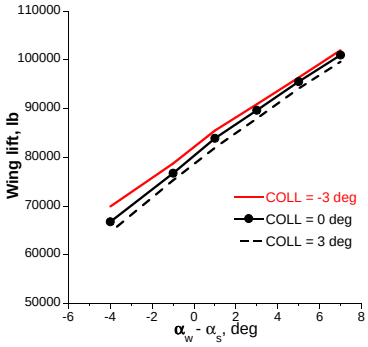

(c) DL = 15, C_W/σ = 0.09, WL = 100

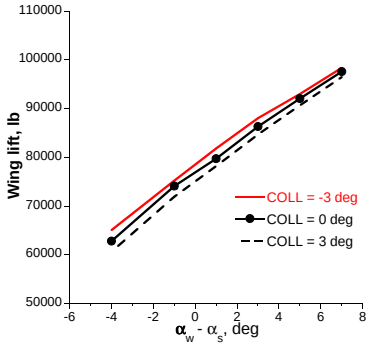

(d) DL = 15, C_W/σ = 0.09, WL = 120

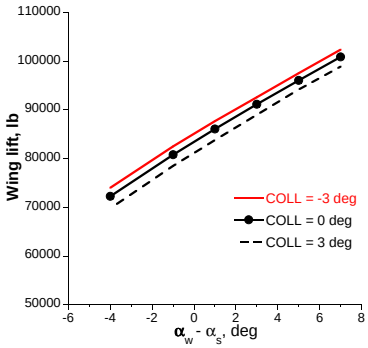

(e) DL = 12, C_W/σ = 0.14, WL = 100

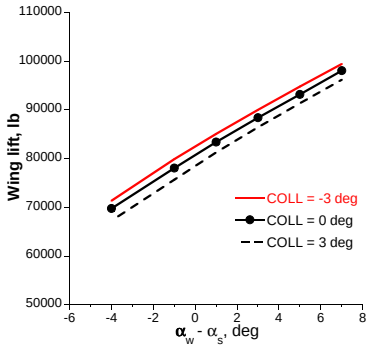

(f) DL = 12, C_W/σ = 0.14, WL = 120

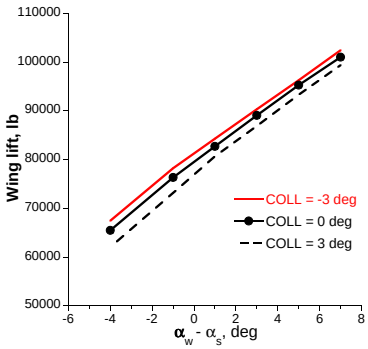

(g) DL = 12, C_W/σ = 0.09, WL = 100

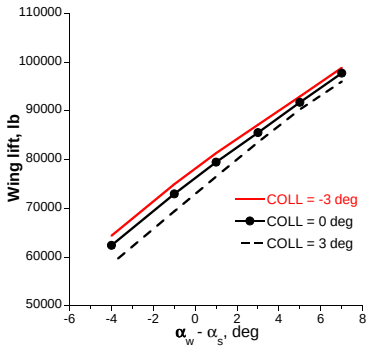

(h) DL = 12, C_W/σ = 0.09, WL = 120

Fig. 9 Wing lift.

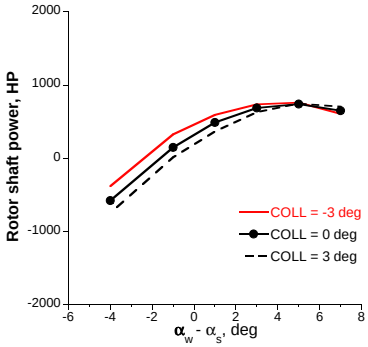

(a) DL = 15, C_W/σ = 0.14, WL = 100

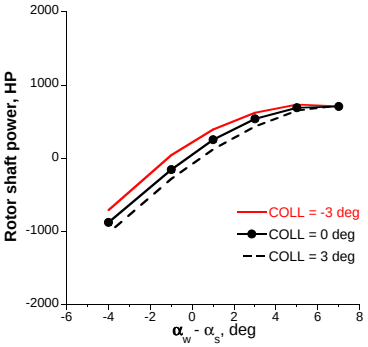

(b) DL = 15, C_W/σ = 0.14, WL = 120

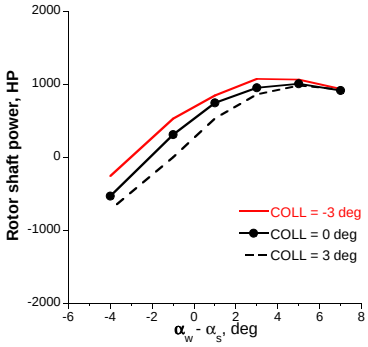

(c) DL = 15, C_W/σ = 0.09, WL = 100

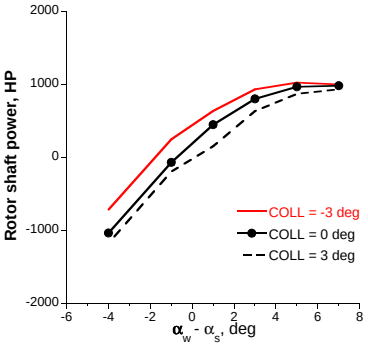

(d) DL = 15, C_W/σ = 0.09, WL = 120

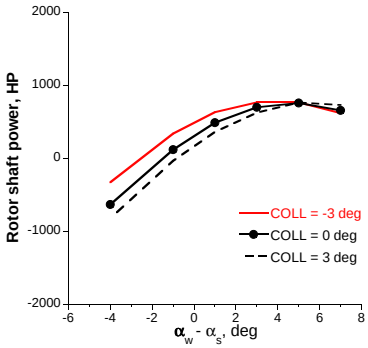

(e) DL = 12, C_W/σ = 0.14, WL = 100

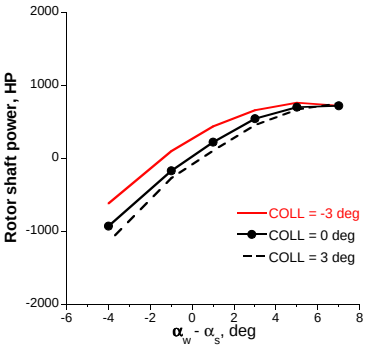

(f) DL = 12, C_W/σ = 0.14, WL = 120

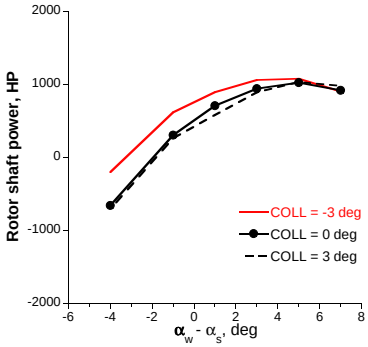

(g) DL = 12, C_W/σ = 0.09, WL = 100

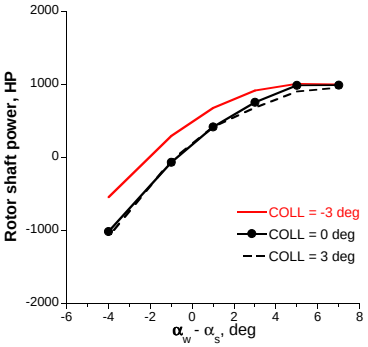

(h) DL = 12, C_W/σ = 0.09, WL = 120

Fig. 10 Rotor shaft power.

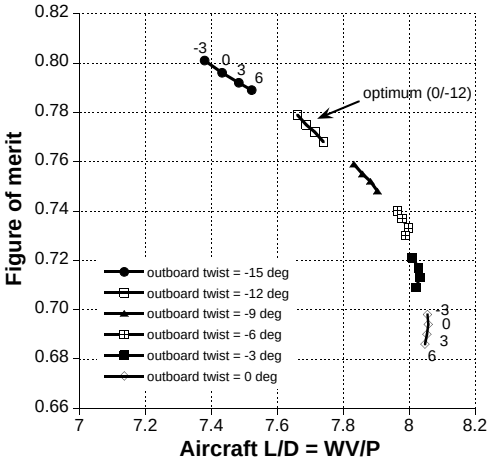

Fig. 11 Effect of blade twist on performance (inboard twist = -3, 0, 3, and 6 deg).

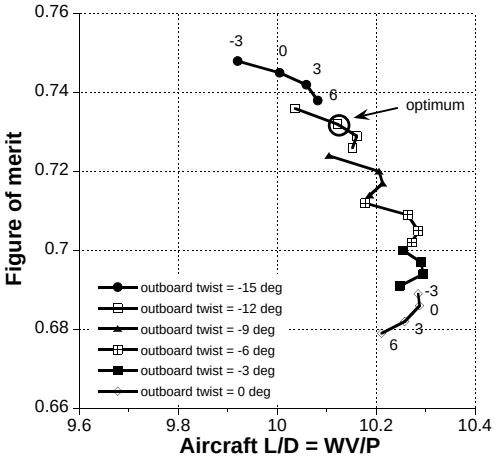

Fig. 12 Effect of blade twist on performance of tandem compound helicopter (inboard twist = -3, 0, 3, and 6 deg) [Ref. 2].

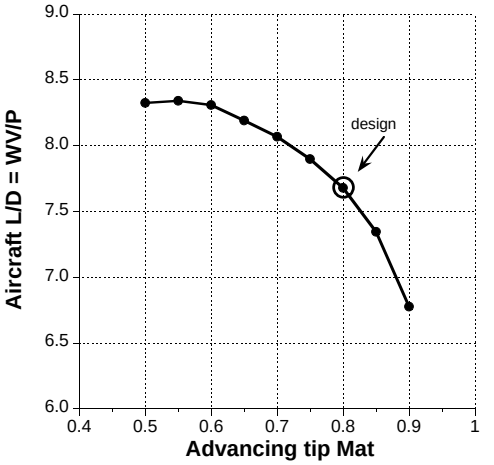

Fig. 13 Effect of tip speed on performance.

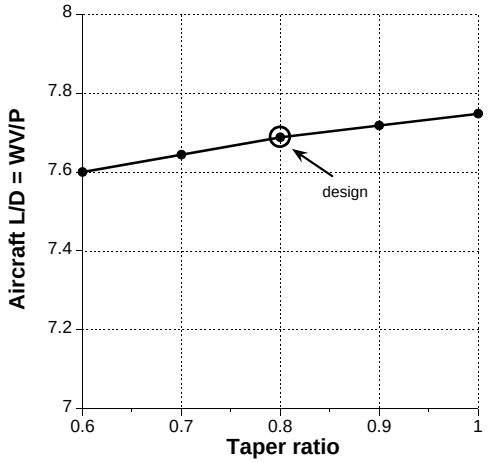

Fig. 14 Effect of blade taper on performance.

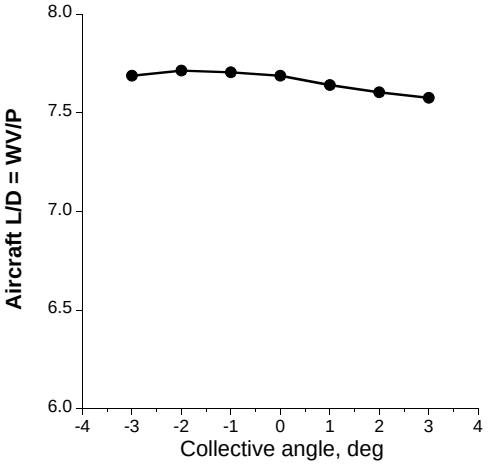

Fig. 15 Effect of collective on performance.

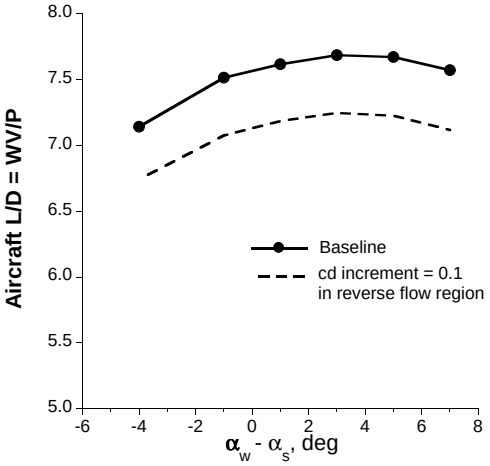

Fig. 16 Effect of airfoil drag on performance.

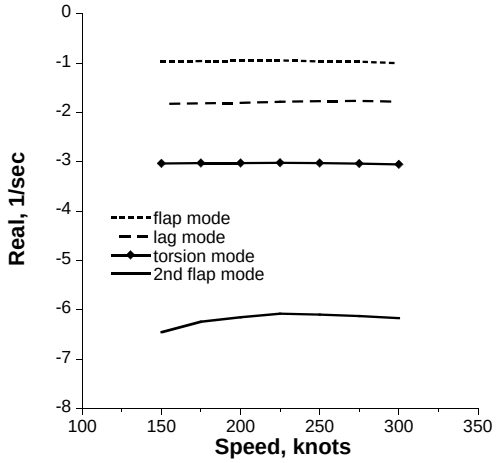

Fig. 17 Cruise stability.

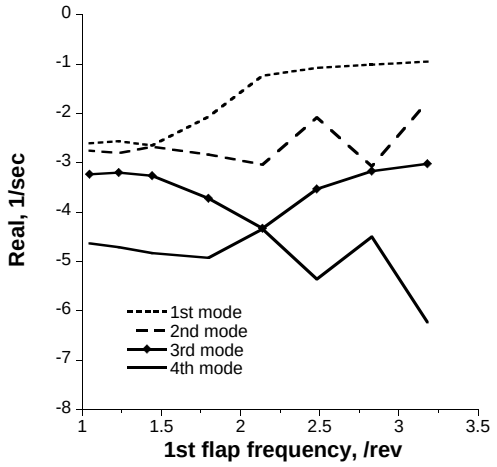

(a) Baseline rotor blade

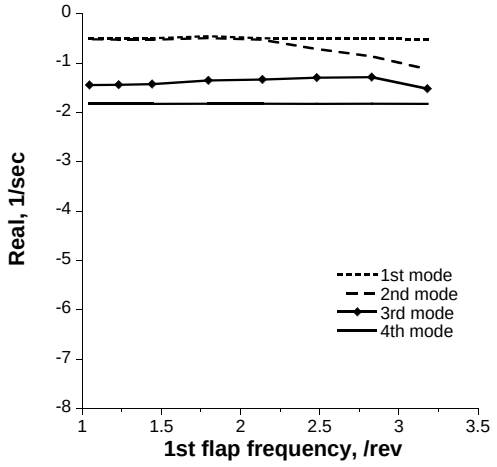

(b) Reduced stiffness (25% GJ & 25% EI_{lag})

Fig. 18 Stability with flap frequency change.

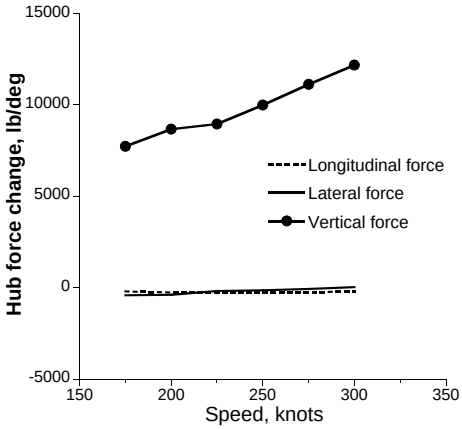

(a) Hub force change w.r.t. collective

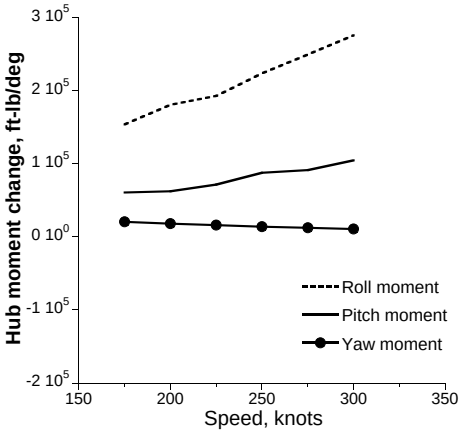

(b) Hub moment change w.r.t. collective

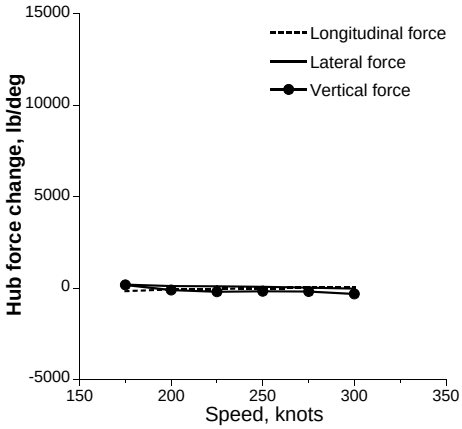

(c) Hub force change w.r.t. lateral cyclic

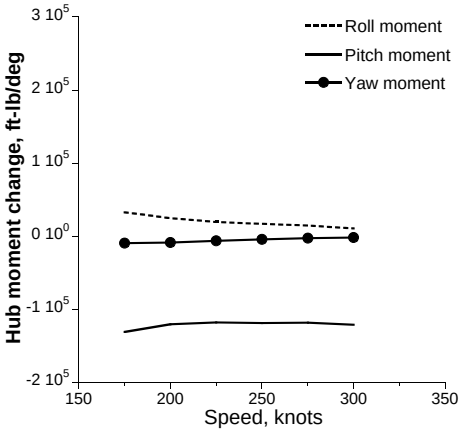

(d) Hub moment change w.r.t. lateral cyclic

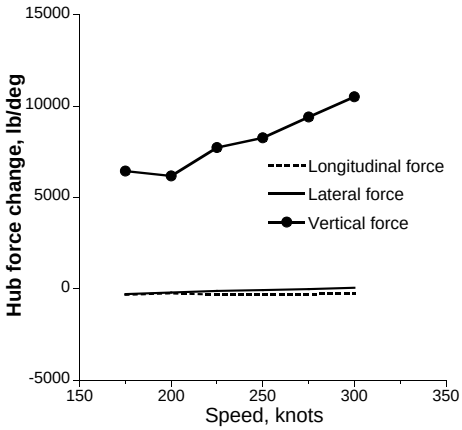

(e) Hub force change w.r.t. longitudinal cyclic

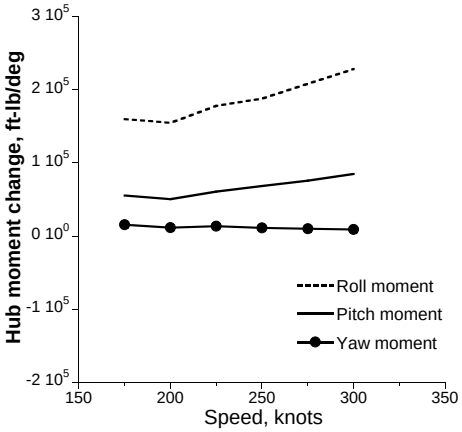

(f) Hub moment change w.r.t. longitudinal cyclic

Fig. 19 Hub load change w.r.t. controls.